

Synthesis, characterization and spectroscopic studies of cyclometalated platinum(II) complexes containing *meta*-bis(2-pyridoxy)benzene

Brenda Ka-Wen Chiu ^a, Michael Hon-Wah Lam ^{a,*}, Derek Yiu-Kin Lee ^a,
Wai-Yeung Wong ^b

^a Department of Biology and Chemistry, City University of Hong Kong, 83 Tat Chee Avenue, Kowloon, Hong Kong, China

^b Department of Chemistry, Hong Kong Baptist University, Waterloo Road, Kowloon Tong, Hong Kong, China

Received 2 February 2004; accepted 3 June 2004

Available online 19 July 2004

Abstract

A series of mononuclear and binuclear cyclometalated platinum(II) complexes containing new terdentate *meta*-bis(2-pyridoxy)benzene ligands: 3,5-bis(2-pyridoxy)toluene (**L₁H**) and 3,5-bis(2-pyridoxy)-2-dodecylbenzene (**L₂H**): [Pt(**L₁**)Cl] (**1**), [Pt(**L₂**)Cl] (**2**), [Pt(**L₁**)(CH₃CN)](ClO₄) (**3**), {[Pt(**L₁**)₂(μ-dppm)](ClO₄)₂ (**4**), {[Pt(**L₂**)₂(μ-dppm)](ClO₄)₂ (**5**), {[Pt(**L₁**)₂(μ-pyrazole)](ClO₄) (**6**), {[Pt(**L₂**)₂(μ-pyrazole)](ClO₄) (**7**), {[Pt(**L₁**)₂(μ-imidazole)](ClO₄) (**8**) and {[Pt(**L₂**)₂(μ-imidazole)](ClO₄) (**9**), have been synthesized and characterized. These ligands are coordinated to platinum(II) in a “pincer”-like manner and the presence of pyridyl donors enhances the availability of the ligand π* orbitals for electronic transition. Spectroscopic properties of these cyclometalated complexes were studied. While the non-coplanar nature of the ligands hinders ligand–ligand and metal–metal interactions in these cyclometalated complexes, the presence of long hydrocarbon side chain on ligand **L₂H** seems to alleviate such hindrance. Intermolecular π–π, and possibly Pt–Pt interactions were observed in complex **2** at high concentration.

© 2004 Elsevier B.V. All rights reserved.

Keywords: Platinum(II) complexes; Pincer ligands; *meta*-Bis(2-pyridoxy)benzene; Cyclometalated complexes; Pt–Pt interactions

1. Introduction

Cyclometalated platinum group metal complexes containing terdentate ligands have aroused considerable research interests in recent years owing to their promising performance as catalysts [1], chemosensors [2] and materials in opto-electronics and luminescent devices [3]. The two most common classes of terdentate ligands for the cyclometalation of transition metals are: (a) “pincer” ligands with the general formula

of [2,6-(*E*CH₂)₂C₆H₄] (where *E* is a neutral two-electron donor, e.g., –NR₂, –PR₂ and –SR) [1c] and (b) conjugated meridional η³-coordinating diiminophenyl and diphenyliminoyl ligands with the general formula of C–N–N, N–C–N and C–N–C (where C represents an aryl ring and N represents an imino moiety) [4,5]. By varying the nature of the electron donors, *E*, electronic properties and reactivity of the metal centre cyclometalated by “pincer” ligands can be fine-tuned. Stereochemistry around the metal centre can also be adjusted by modifying substituents on *E* and, sometimes, on the aryl ring. These features are particularly desirable in the design of organometallic catalysts. For the conjugated diiminophenyl and diphenyliminoyl ligands, the availability of the low lying π*

* Corresponding author. Tel.: +852-2788-7329; fax: +852-2788-7406.

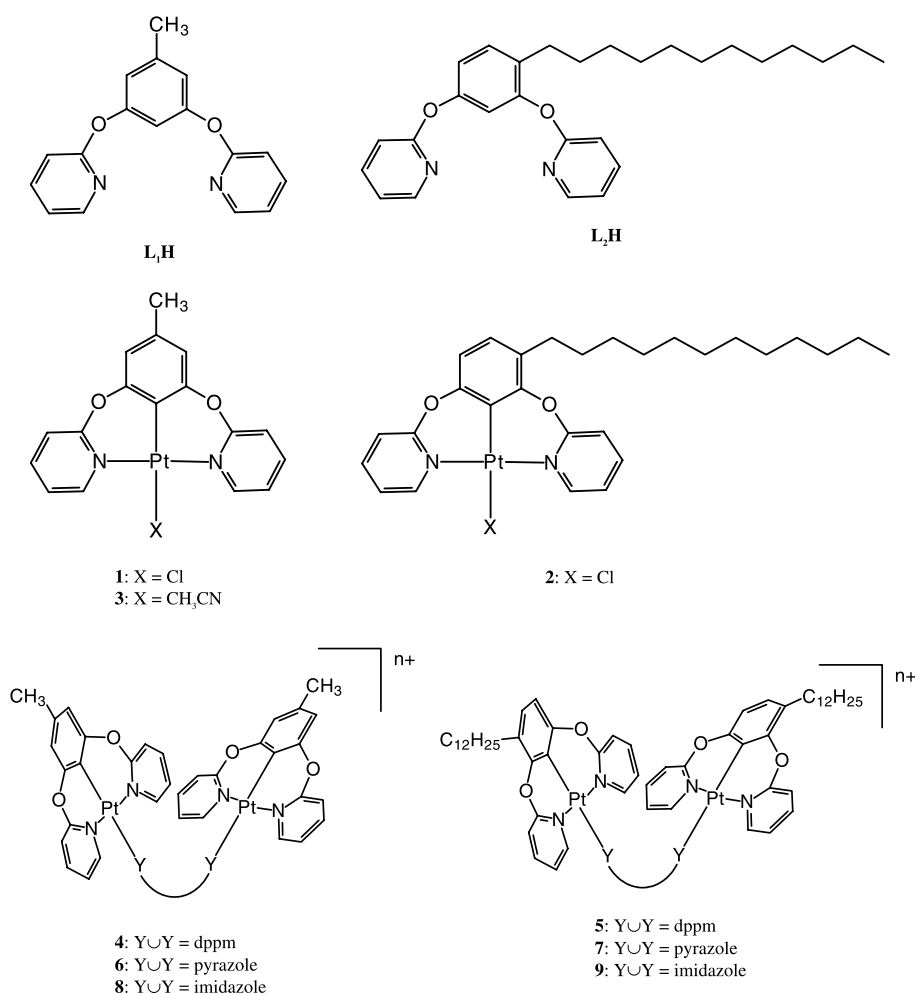
E-mail address: bhmhwlam@cityu.edu.hk (M.H.-W. Lam).

orbitals of the ligands for participation in electronic transition has given rise to many interesting spectroscopic and luminescent properties of the resultant cyclometalated complexes [6]. It would be interesting to study the properties of cyclometalated metal complexes containing terdentate chelating ligands with both features of “pincer”-type ligands and conjugated CNN/NCN/CNC ligands. In this work, we report the synthesis of two substituted *meta*-bis(2-pyridoxy)benzene (**L₁H** and **L₂H**) which are able to coordinate, in “pincer”-like manner, with platinum(II) to form a series of mononuclear and binuclear cyclometalated NCN Pt(II) complexes (**1–9**) (Scheme 1). Special attention is given to the spectroscopic properties of these new cyclometalated Pt(II) complexes as the presence of pyridyl donors enhances the availability of the ligand π^* orbitals for electronic transition while the “pincer”-like arrangement of the ligands de-conjugates the three aromatic rings by ether spacers and hinders intramolecular π – π and metal–metal interactions in the binuclear cyclometalated NCN Pt(II) complexes.

2. Results and discussion

2.1. Synthesis and characterization of ligands and cyclometalated complexes

The substituted *m*-bis(2-pyridoxy)benzenes **L₁H** and **L₂H** were obtained in gram-scale by a one-pot synthetic approach [7] from substituted resorcinol and 2-bromopyridine. Mononuclear cyclometalated NCN Pt(II) complexes [Pt(**L₁**)Cl] (**1**) and [Pt(**L₂**)Cl] (**2**) were obtained by reacting the corresponding *m*-bis(2-pyridoxy)benzene with one equivalent of $K_2[PtCl_4]$ in refluxing acetic acid. Lability of chloride *trans*- to the Pt–C σ bond was demonstrated by its ease of substitution by acetonitrile to generate [Pt(**L₁**)(CH₃CN)]⁺ (**3**). This is attributable to the strong *trans*-effect of the cyclometalated aryl ring [8]. The binuclear complexes **4–9** were synthesized by reacting the mononuclear cyclometalated NCN Pt(II) complexes with either dppm or deprotonated pyrazole and imidazole (by potassium *tert*-butoxide) in CH₃CN/CH₃OH mixture under an



Scheme 1. The *meta*-bis(2-pyridoxy)benzene ligands and cyclometalated Pt(II) complexes synthesized.

inert atmosphere. All the ligands and cyclometalated NCN Pt(II) complexes were characterized by ES-MS and ^1H NMR spectrometry. X-ray crystal structures were determined for complexes **1**, **3**, **6** and **8**. Selected bond lengths and angles as well as dihedral angles between aromatic rings of the complexes are tabulated in Tables 1 and 2.

Perspective view of the crystal structure of the neutral complex **1**, with atom and ring labelling, is shown in Fig. 1. The 3,5-bis(2-pyridoxy)toluene ligand L_1 is coordinated to the platinum(II) centre via its two pyridyl-*N* and one aryl-*C* in a terdentate manner. The Pt(II) centre adopts a square planar coordination geometry with bond angles N(1)–Pt(1)–N(2) and C(6)–Pt(1)–Cl(1) of $175.6(4)^\circ$ and $179.5(4)^\circ$, respectively. The bond distances between Pt(II) and the pyridyl-*N*, Pt(1)–N(1) and Pt(1)–N(2), were 2.032(9) and 2.033(10) Å, respectively. These are shorter than those observed in typical Pt(II) complexes of “NCN” pincer-type ligands with either N(sp³) or N(sp²) donors [4c,9], but are very similar to those observed in a related cyclometalated Pt(II) complex containing a conjugated 1,3-bis(2-pyridyl)benzene (NCN) ligand [4c]. On the other hand, the bond distance of 1.959(14) Å between the Pt(II) centre and the aryl-*C*, Pt(1)–C(6), is longer than the corresponding bond distance of 1.907(8) Å in the cyclometalated Pt(II) 1,3-bis(2-pyridyl)benzene complex [4c], but lies in a similar range of most of the reported Pt(II) complexes of “NCN” pincer-type ligands. The Pt(1)–Cl(1) bond distance is 2.419(3) Å. As the three aromatic rings of the ligand are de-conjugated, the three rings in complex **1** are not co-planar with each other. Dihedral angles between the pyridyl rings and the aryl ring are 42.7° and 32.0° . Perspective view of the crystal structure of complex **3**, with atom and ring labelling, is shown in Fig.

2. The cationic complex **3** was obtained by the substitution of chloride *trans*- to the Pt–C σ bond in complex **1** by acetonitrile. The Pt(II) to pyridyl-*N* and Pt(II) to aryl-*C* bond distances are comparable to those in complex **1** (Pt(1)–N(1): 2.027(7) Å; Pt(1)–N(2): 2.030(7) Å; Pt(1)–C(11): 1.965(9) Å). The bond distance between Pt(II) and acetonitrile-*N* is 2.087(7) Å. The aryl ring makes dihedral angles of 35.8° and 34.2° with the N(1)- and N(2)-pyridyl rings, respectively.

Perspective view of the crystal structure of the cationic binuclear complex **6**, with atom and ring labelling, is shown in Fig. 3. The two cyclometalated [Pt(L_1)] units are bridged by a deprotonated pyrazole via N(3) and N(4). Within each cyclometalated [Pt(L_1)] unit, the Pt(II) centre adopts a square planar coordination geometry with the pyridyl-*N*–Pt(II)–pyridyl-*N'* bond angle of $176.54(16)$ – $175.81(16)^\circ$ and the aryl-*C*–Pt(II)–pyrazolyl-*N* bond angle of $177.57(18)$ – $178.68(18)^\circ$. The Pt(II) to pyridyl-*N* and Pt(II) to aryl-*C* bond distances are 2.023(4)–2.038(4) and 1.954(4)–1.974(5) Å, respectively. These bond distances are comparable to those observed in the mononuclear complex **1** and **3**. The Pt(II) to pyrazolyl-*N* bond distance is 2.098(4)–2.113(4) Å and is in accordance with that observed in $\{[\text{Pt}(\text{L})]_2(\mu\text{-pyrazole})\}^+$ (L = 6-phenyl-2,2'-bipyridine), where the Pt(II)–pyrazolyl-*N* bond distance is 2.009(4) Å [6d]. The aryl and pyridyl rings of the cyclometalating ligands in the binuclear complex are also deviated from co-planarity as in the mononuclear complex **1**. Dihedral angles between the pyridyl rings lie in the range 63.5 – 63.6° whereas those between the pyridyl rings and the aryl ring in the range 35.4 – 48.9° . The intramolecular Pt–Pt distance in the binuclear complex is 3.876 Å, which is much longer than those in the related binuclear Pt(II)

Table 1

Selected bond distances (Å), bond angles ($^\circ$) and dihedral angles between aromatic rings ($^\circ$) of [Pt(L_1)Cl] (**1**) and [Pt(L_1)(CH₃CN)](ClO₄) (**3**)

<i>[Pt(L₁)Cl] (1)</i>			
Pt(1)–C(6)	1.959 (14)	Pt(1)–Cl(1)	2.419 (3)
Pt(1)–N(1)	2.032 (9)	Pt(1)–N(2)	2.033 (10)
C(6)–Pt(1)–Cl(1)	179.5 (4)	N(1)–Pt(1)–N(2)	175.6 (4)
C(6)–Pt(1)–N(1)	88.5 (5)	C(6)–Pt(1)–N(2)	87.7 (6)
C(1)–O(1)–C(11)	119.1 (11)	C(13)–O(2)–C(7)	123.5 (11)
Ring A–Ring B	42.7	Ring B–Ring C	32.0
<i>[Pt(L₁)(CH₃CN)](ClO₄) (3)</i>			
Pt(1)–C(11)	1.965 (9)	Pt(1)–N(2)	2.030 (7)
Pt(1)–N(1)	2.027 (7)	Pt(1)–N(3)	2.087 (7)
C(11)–Pt(1)–N(3)	176.8 (3)	N(1)–Pt(1)–N(2)	177.6 (3)
C(11)–Pt(1)–N(1)	88.6 (3)	C(11)–Pt(1)–N(2)	89.6 (3)
C(5)–O(1)–C(6)	121.6 (7)	C(13)–O(2)–C(10)	124.6 (7)
Ring A–Ring B	35.8	Ring B–Ring C	34.2

Table 2

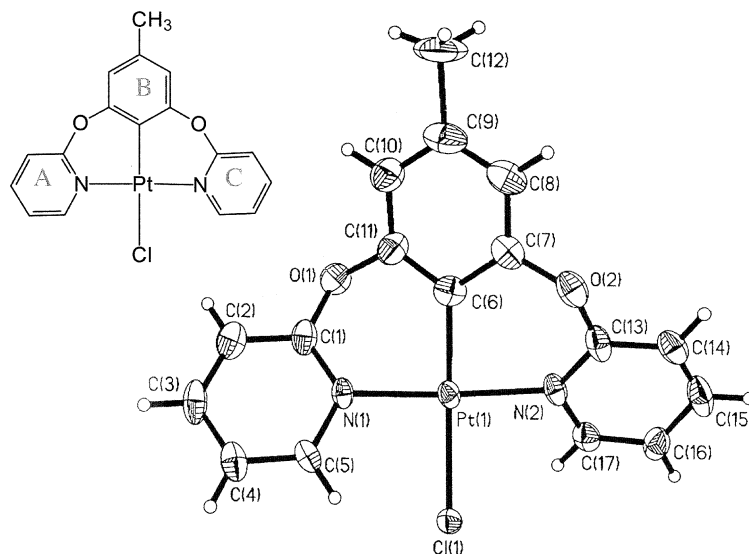
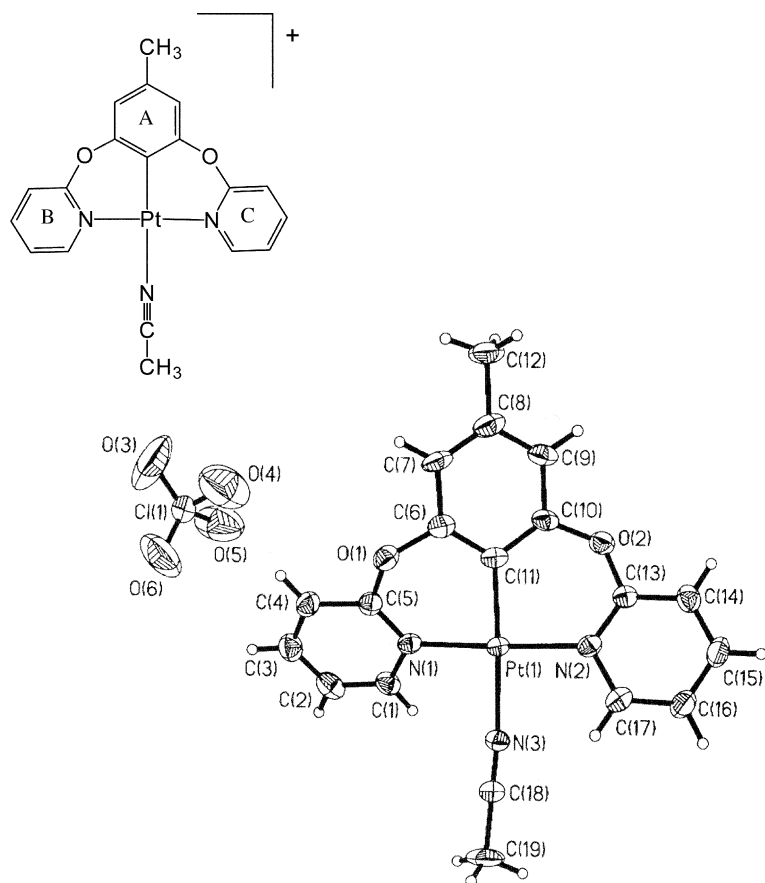
Selected bond distances (Å), bond angles (°) and dihedral angles between aromatic rings (°) of $\{[Pt(L_1)]_2(\mu\text{-pyrazole})\}(ClO_4)$ (**6**) and $\{[Pt(L_1)]_2(\mu\text{-imidazole})\}(ClO_4)$ (**8**)

$\{[Pt(L_1)]_2(\mu\text{-pyrazole})\}(ClO_4)$ (6)			
C(7)–Pt(1)	1.954 (4)	C(27)–Pt(2)	1.974 (5)
N(1)–Pt(1)	2.037 (4)	N(5)–Pt(2)	2.023 (4)
N(2)–Pt(1)	2.027 (4)	N(6)–Pt(2)	2.038 (4)
N(3)–Pt(1)	2.098 (4)	N(4)–Pt(2)	2.113 (4)
C(7)–Pt(1)–N(3)	177.57 (18)	C(27)–Pt(2)–N(4)	178.68 (18)
N(1)–Pt(1)–N(2)	176.54 (16)	N(5)–Pt(2)–N(6)	175.81 (16)
C(7)–Pt(1)–N(1)	88.80 (18)	C(27)–Pt(2)–N(5)	87.90 (17)
C(7)–Pt(1)–N(2)	88.13 (18)	C(27)–Pt(2)–N(6)	87.94 (18)
N(1)–Pt(1)–N(3)	91.61 (15)	N(5)–Pt(2)–N(4)	92.67 (15)
N(2)–Pt(1)–N(3)	91.53 (15)	N(6)–Pt(2)–N(4)	91.48 (16)
C(5)–O(1)–C(6)	120.9 (4)	C(26)–O(3)–C(25)	122.1 (4)
C(8)–O(2)–C(13)	122.1 (4)	C(28)–O(4)–C(33)	117.0 (4)
Ring A–Ring B	39.9	Ring A–Ring C	63.6
Ring A–Ring D	50.2	Ring B–Ring C	35.4
Ring B–Ring D	38.0	Ring C–Ring D	71.5
Ring D–Ring E	70.4	Ring D–Ring F	34.9
Ring D–Ring G	65.1	Ring E–Ring F	37.5
Ring E–Ring G	63.5	Ring F–Ring G	48.9
Ring C–Ring E	16.7		
$\{[Pt(L_1)]_2(\mu\text{-imidazole})\}(ClO_4)$ (8)			
C(11)–Pt(1)	1.986 (10)	C(31)–Pt(2)	1.976 (11)
N(1)–Pt(1)	2.043 (9)	N(5)–Pt(2)	2.030 (9)
N(2)–Pt(1)	2.023 (8)	N(6)–Pt(2)	2.039 (10)
N(3)–Pt(1)	2.082 (8)	N(4)–Pt(2)	2.097 (8)
C(11)–Pt(1)–N(3)	178.8 (4)	C(31)–Pt(2)–N(4)	178.9 (4)
N(1)–Pt(1)–N(2)	177.5 (3)	N(5)–Pt(2)–N(6)	177.9 (3)
C(11)–Pt(1)–N(1)	88.9 (4)	C(31)–Pt(2)–N(5)	89.0 (4)
C(11)–Pt(1)–N(2)	88.6 (4)	C(31)–Pt(2)–N(6)	89.0 (4)
N(1)–Pt(1)–N(3)	90.1 (3)	N(5)–Pt(2)–N(4)	90.5 (3)
N(2)–Pt(1)–N(3)	92.4 (3)	N(6)–Pt(2)–N(4)	91.4 (3)
C(6)–O(1)–C(5)	121.9 (9)	C(26)–O(3)–C(25)	122.8 (8)
C(10)–O(2)–C(13)	121.7 (8)	C(30)–O(4)–C(33)	121.3 (9)
Ring A–Ring B	40.1	Ring A–Ring C	58.8
Ring A–Ring D	59.8	Ring B–Ring C	31.2
Ring B–Ring D	33.3	Ring C–Ring D	58.7
Ring D–Ring E	75.0	Ring D–Ring F	44.2
Ring D–Ring G	60.4	Ring E–Ring F	34.9
Ring E–Ring G	60.2	Ring F–Ring G	38.0

cyclometalated complexes, e.g., 3.081 Å in $\{[Pt(tpy)]_2(\mu\text{-guanidine})\}^{3+}$ [10], 3.270 Å in $\{[Pt(L)]_2(\mu\text{-dppm})\}^{2+}$ [11], 3.432 Å in $\{[Pt(tpy)]_2(\mu\text{-pyrazole})\}^{3+}$ [12] and 3.612 Å in $\{[Pt(L)]_2(\mu\text{-pyrazole})\}^+$ [6d] (where tpy = terpyridine; L = 6-phenyl-2,2'-bipyridine). Such a long intramolecular Pt–Pt distance is probably caused by the steric hindrance of the two non-coplanar cyclometalated ligands. This also implies the absence of any metal–metal interaction in the binuclear complex as it has been proposed that the upper limit of intramolecular Pt–Pt distance for metal–metal interaction is ~ 3.6 Å [6d]. The lack of metal–metal interaction in the binuclear complex **6** has also been demonstrated spectroscopically and will be dis-

cussed later. The torsion angle about the Pt(1)–Pt(2) axis is 14.3°.

Perspective view of the crystal structure of the cationic binuclear complex **8**, with atom and ring labelling, is shown in Fig. 4. The two cyclometalated $[Pt(L_1)]$ units are bridged by a deprotonated imidazole. Bridging via the imidazolium-N (N(3) and N(4)) or imidazolium-C (C(18) and C(20)) are possible and X-ray crystallography may not be able to distinguish the two possibilities. Nevertheless, 1H NMR of **8** did not contain any highly downfield protons in the range 12–14 ppm corresponding to imidazolium N–H [13]. Thus, it is reasonable to assign the structure of **8** as μ -imidazolyl cyclometalated Pt(II) dimer bridged via N(3) and N(4) of the imidazo-

Fig. 1. Perspective view of $[\text{Pt}(\text{L}_1)\text{Cl}]$ (**1**).Fig. 2. Perspective view of $[\text{Pt}(\text{L}_1)(\text{CH}_3\text{CN})](\text{ClO}_4)$ (**3**).

lium ring. As in complex **6**, the Pt(II) centres are also in square planar coordination geometry with the pyridyl-*N*–Pt(II)–pyridyl-*N'* bond angle of 177.5(3)–177.9(3)° and the aryl-*C*–Pt(II)–imidazolium-*N* bond angle of 178.8(4)–178.9(4)°. The Pt(II) to pyridyl-*N* and Pt(II)

to aryl-*C* bond distances are 2.023(8)–2.043(9) and 1.976(11)–1.986(10) Å, respectively. The Pt(II) to imidazolium-*N* bond distance is 2.082(8)–2.097(8) Å. These bond distances are comparable to those observed in the μ -pyrazole bridged binuclear complex **6**. Within each

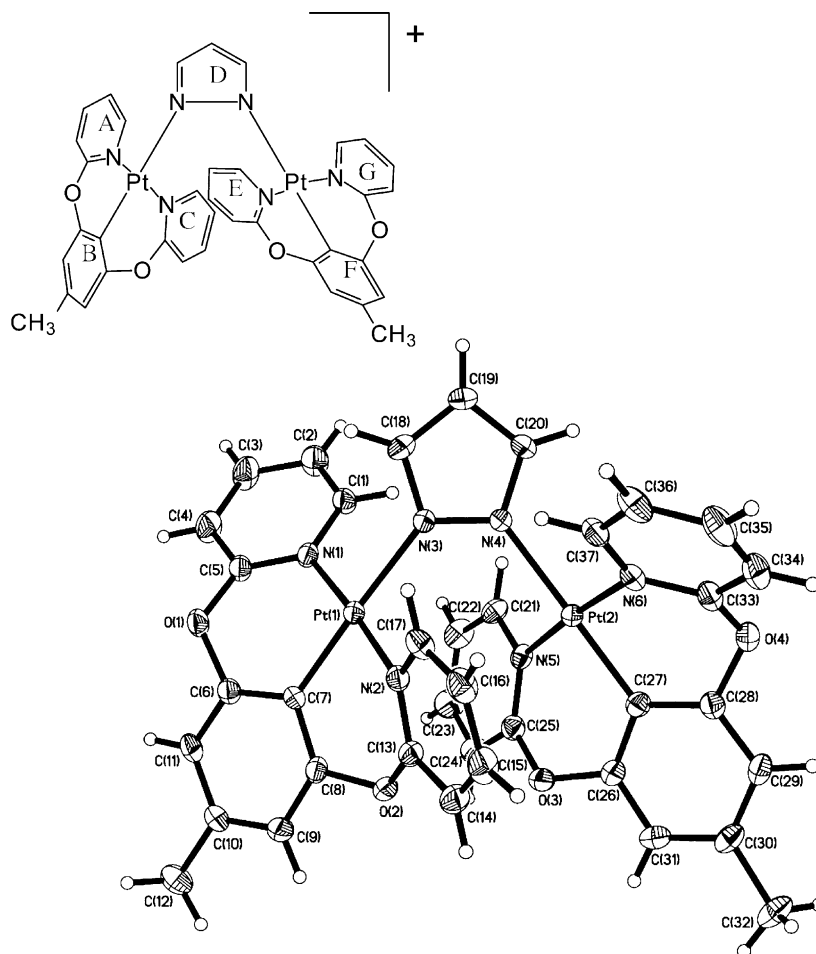


Fig. 3. Perspective view of the cation of $\{[Pt(L_1)]_2(\mu\text{-pyrazole})\}(\text{ClO}_4)$ (**6**).

$[Pt(L_1)]$ unit, the dihedral angles between the two pyridyl rings range from 58.8° to 60.2° . The dihedral angles between the pyridyl rings and the aryl ring are $31.2\text{--}40.1^\circ$.

Structures of the mononuclear and binuclear cyclometalated Pt(II) complexes containing the 3,5-bis(2-pyridoxy)-2-dodecylbenzene ligand L_2 are expected to resemble those of the related complex **1**, **3**, **6** and **8**. However, all attempts to obtain X-ray quality crystals of complexes **2**, **5**, **7** and **9** were not successful.

2.2. Spectroscopic and luminescent properties of the cyclometalated complexes

Table 3 summarizes the electronic transition and luminescent properties of the ligands as well as the mononuclear and binuclear cyclometalated NCN Pt(II) complexes. By comparing with the UV–Vis absorption characteristics of ligands L_1H and L_2H as well as those of related cyclometalated Pt(II) complexes with conjugated 6-phenyl-2,2'-bipyridine (CNN) and 2,6-diphenylpyridine (CNC) ligands [6d,14], the high energy transitions ($\lambda < 300$ nm) of the cyclometalated complexes are attributable to intraligand $\pi \rightarrow \pi^*$ transitions while

those in the region 300–340 nm are likely to be $^1\text{MLCT Pt}(d\pi) \rightarrow L(\pi^*)$ in nature. The latter are of much higher energy compared to those $^1\text{MLCT}$ transitions in cyclometalated Pt(II) complexes with conjugated terdentate ligands (λ_{max} in the range 400–440 nm) [11]. This is most probably caused by the de-conjugated nature of the present NCN ligands where $L(\pi^*)$ are expected to be of higher energy than those in conjugated terdentate ligands. Room temperature solution emission spectra of most of the mononuclear and binuclear cyclometalated NCN Pt(II) complexes are dominated by ligand centred $\pi^* \rightarrow \pi$ transition at 440–460 nm. At higher concentration (1×10^{-3} M), ligand L_2H shows an additional lower energy emission peak at 530 nm. This is probably caused by intermolecular $\pi\text{--}\pi$ interaction at high concentration, aided by the dodecyl sidearm on L_2H , which lowers the $\pi\pi^*$ energy gap. No such intermolecular interaction is observed in ligand L_1H up to a concentration of 1×10^{-2} M. Solution emission properties of mononuclear complex **2** also show evidence of ligand–ligand $\pi\text{--}\pi$ and possibly $d^8\text{--}d^8$ interaction at high concentration. At 1×10^{-2} M in CHCl_3 , intensity of the original ligand centred $\pi^* \rightarrow \pi$ emission is diminished and an in-

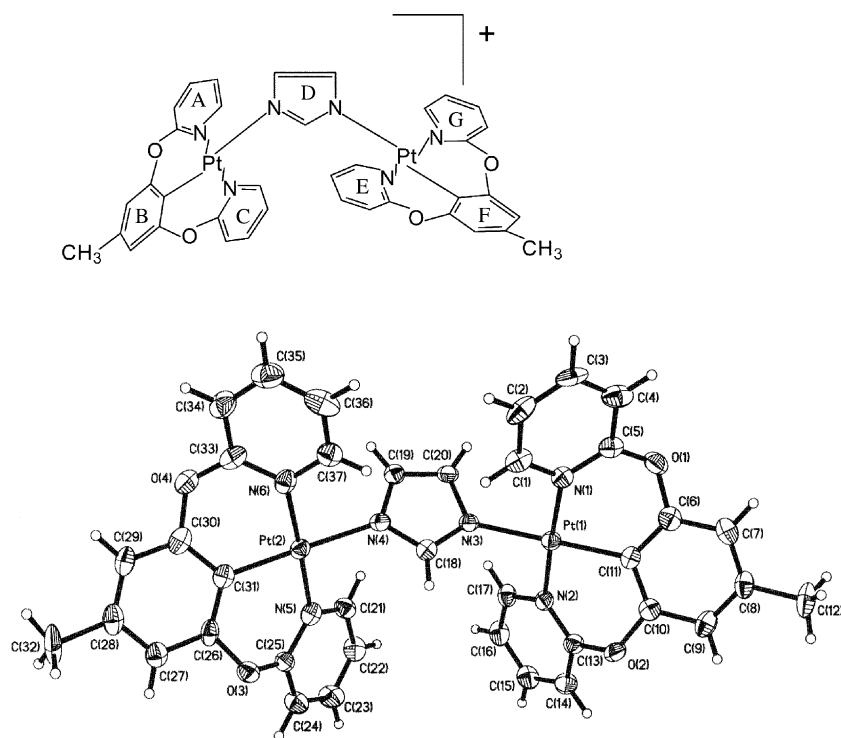


Fig. 4. Perspective view of the cation of $\{Pt(L_1)_2\}(\mu\text{-imidazole})(ClO_4)$ (**8**).

Table 3

Electronic transition and luminescent properties of all the mononuclear and binuclear cyclometalated NCN Pt(II) complexes

Ligand/complex	Solvent	UV–Vis absorption spectra ^a $\lambda_{\text{max}}/\text{nm}$ ($\epsilon/\text{dm}^3 \text{mol}^{-1} \text{cm}^{-1}$)	Solution emission spectra ^b $\lambda_{\text{max}}/\text{nm}$ (λ_{ex} at 360 nm)
L₁H	CHCl ₃	251 (38,000), 276 (30,890)	450 ^a
L₂H	CHCl ₃	252 (37,410), 275 (31,140)	440 ^a , 530 ^c
1	CHCl ₃	241 (32,501), 311 (7704)	440 ^a
	CH ₃ CN	282 (5974), 301 (4378), 330 (1629)	445 ^a
2	CHCl ₃	241 (17,921), 307 (1974)	455 ^a , 555 ^c
3	CH ₂ Cl ₂	231 (41,055), 290 (9889)	385 ^a
	CH ₃ CN	220 (13,120), 245 (8 014), 300 (1798)	444 ^a
4	CHCl ₃	241 (31,556), 313 (11,170)	450 ^a
	CH ₃ CN	221 (25,705), 272 (11,976), 310 (4080) sh	445 ^a
5	CHCl ₃	241 (34,037), 268 (18,241) sh, 312 (4589) sh	460 ^a , 530 ^c
6	CHCl ₃	243 (42,218), 292 (12,926) sh, 335 (6720) sh	450 ^a
	CH ₃ CN	221 (31,625), 242 (24,847) sh, 286 (3328), 321 (5541)	450 ^a
7	CHCl ₃	275 (40,529), 405 (1059)	450 ^a
8	CHCl ₃	241 (38,816), 287 (8894), 303 (7054) sh, 332 (2814) sh	465 ^a
	CH ₃ CN	249 (47,570), 272 (47,402), 332 (4075) sh	466 ^a
9	CHCl ₃	240 (38,178), 277 (19,938), 336 (2852) sh	445 ^a

^a Concentration = $1.0 \times 10^{-5} \text{ mol dm}^{-3}$.

^b At 298 K.

^c Concentration = $1.0 \times 10^{-2} \text{ mol dm}^{-3}$.

tense new lower energy emission peak at λ_{max} 555 nm is observed (Fig. 5). The red-shift of the emission peak from 530 to 555 nm indicates extra interaction between mononuclear units of **2** at high concentration in addition to the intermolecular ligand–ligand π – π interaction. Metal–metal interaction similar to those observed in square planar Pt(II) complexes with conjugated copla-

nar terdentate ligands [15] is possible. Again, the long carbon chain on ligand **L₂** seems to facilitate these ligand–ligand and metal–metal interactions as no lower energy emission peak is observed in complex **1** (an analog of **2** without the long carbon chain on the ligand) even at high concentration. Unlike many binuclear cyclometalated Pt(II) complexes with conjugated CNN and

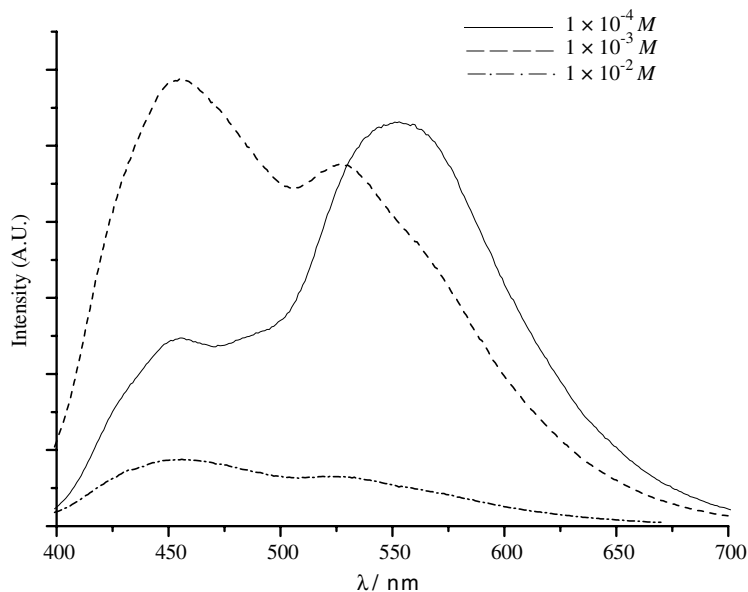


Fig. 5. Emission spectra of complex **2** at different concentrations in CHCl_3 at 298 K.

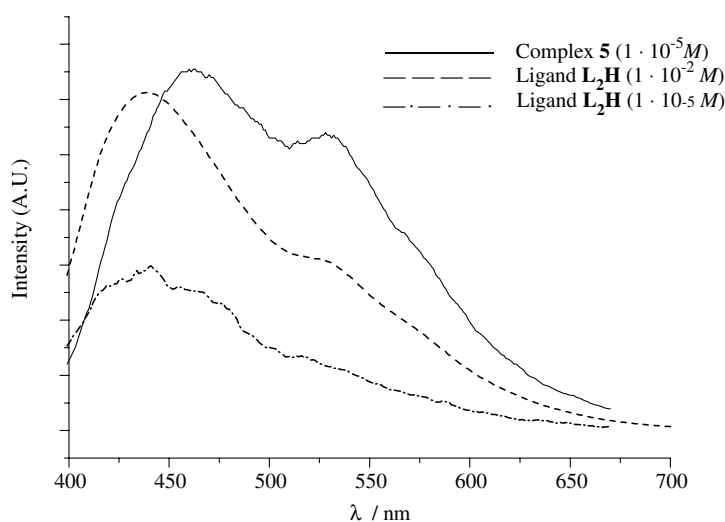


Fig. 6. Emission spectrum of binuclear complex **5** ($1 \times 10^{-5} \text{ M}$) compared with those of ligand **2** at the same and higher concentrations in CHCl_3 at 298 K.

CNC ligands [6d,14], no intramolecular d^8-d^8 and/or $\pi-\pi$ interaction in the binuclear complexes **4** and **6–9** is apparent. Long intramolecular Pt–Pt distance for the absence of any metal–metal interaction is observed in the crystal structure of complex **6**. Lower energy emission peak likely to be caused by intramolecular ligand–ligand $\pi-\pi$ interaction is also absent. This is attributable to the distortion of the “pincer”-like ligands from co-planarity which hinders any close interaction between the cyclometalated NCN Pt(II) units in the binuclear complexes. There is, on the other hand, spectroscopic evidence that shows the existence of intramolecular $\pi-\pi$ interaction between the cyclometalated Pt(II) units in the μ -dppm bridged binuclear complex **5**. At low concentration ($1 \times 10^{-5} \text{ M}$) in CHCl_3 , a low energy emission peak at

530 nm similar to that appeared in the emission spectrum of ligand **L₂H** at much higher concentration is observed (Fig. 6). The analogous pyrazole-bridged binuclear complex **7** does not show any lower energy emission peak even at high concentration. This may be due to the coordination geometry of the pyrazole-bridge which is unable to bring the two cyclometalated NCN Pt(II) units close enough for interaction as in the μ -dppm bridged complex **5**.

3. Conclusion

A series of mononuclear and binuclear cyclometalated Pt(II) complexes containing *m*-bis(2-pyridoxy)ben-

zenes as terdentate cyclometalation NCN ligands have been synthesized and characterized. The *m*-bis(2-pyridoxy)benzenes were able to cyclometalate Pt(II) in a “pincer”-like manner. The non-coplanar nature of the cyclometalation ligands hinders inter- and intramolecular ligand–ligand and metal–metal interactions in mononuclear and binuclear complexes. The presence of long carbon side chain on the ligand (as in ligand **L**₂) seems to alleviate such hindrance. Intermolecular π – π , and possibly d^8 – d^8 , interactions are observed in the mononuclear cyclometalated complex **2** at high solution concentration. X-ray structure and spectroscopic characteristics of the binuclear complexes with different bridging moieties (μ -imidazolyl, μ -pyrazolyl and μ -dppm) indicate the absence of intramolecular interaction between the cyclometalated NCN Pt(II) mononuclear units, except in complex **5** where the combination of the μ -dppm bridge which is known to be able to effect close proximity of mononuclear units and the presence of the dodecyl side chain on the ligand is likely to bring about intramolecular π – π interaction.

4. Experimental

4.1. General

Potassium tetrachloroplatinate(II), resorcinol, 4-dodecylresorcinol, 2-bromopyridine, pyrazole, imidazole and bis(diphenylphosphino)methane (dppm) were purchased from Aldrich. All solvents used were of analytical reagent grade and were from Riedel-de Harn, Lab-Scan Analytical Sciences and BDH. ¹H NMR spectra were measured by a Varian YH300 300 MHz Superconducting Magnet High Field NMR spectrometer with tetramethylsilane used as internal reference. UV–Vis spectra were measured by a Hewlett–Packard 8425A ultra-violet diode-array spectrophotometer. Luminescent spectra were measured by a Fluoromax-3 spectrofluorometer. Electrospray mass spectra were measured by a PE SCIEX API 365 LC/MS/MS system.

4.2. Synthesis of 3,5-bis(2-pyridoxy)toluene (**L**₁**H**)

A mixture of orcinol (3.0 g, 24.2 mmol) and 2-bromopyridine (7.65 g, 48.4 mmol) was heated until orcinol melted. Potassium carbonate (6.68 g, 48.4 mmol) was then added and the mixture was further heated at 200–210 °C for 3 h. The resulting tar was extracted several times with dichloromethane and the extracts combined and evaporate to dryness to give crude 3,5-bis(2-pyridoxy)toluene (**L**₁**H**). The product (2.8 g, 42% yield) was purified by silica gel column chromatography using dichloromethane as eluent. ¹H NMR (CDCl₃, 300 MHz) δ : 8.21 (dd, 2H, pyridoxy-H), 7.68 (td, 2H, pyridoxy-H), 7.00 (td, 2H, pyridoxy-H), 6.93 (s, 1H, tolyl-H), 6.90 (s,

1H, tolyl-H), 6.80 (d, 2H, pyridoxy-H), 6.74 (s, 1H, tolyl-H), 2.36 (s, 3H, tolyl-CH₃). ES-MS (CH₂Cl₂, +ve mode): 279 [M]⁺.

4.3. Synthesis of 3,5-bis(2-pyridoxy)-2-dodecylbenzene (**L**₂**H**)

3,5-Bis(2-pyridoxy)-2-dodecylbenzene (**L**₂**H**) was obtained from 4-dodecylresorcinol (6.74 g, 24.2 mmol) in a similar way as **L**₁**H**. Yield 6.0 g, 57%. ¹H NMR (CDCl₃) δ : 8.16 (m, 2H, pyridoxy-H), 7.64 (td, 2H, pyridoxyl-H), 7.24 (d, 2H, pyridoxyl-H), 6.95 (m, 2H, pyridoxyl-H), 6.90 (s, 1H, aryl-H), 6.87 (d, 1H, aryl-H), 6.83 (d, 1H, aryl-H), 1.24 (m, 25H, –C₁₂H₂₅). ES-MS (Ether/THF, +ve mode): 433 [M]⁺.

4.4. Synthesis of [Pt(**L**₁)Cl] (**1**)

K₂[PtCl₄] (1.66 g, 4.0 mmol) was suspended in a glacial acetic acid solution (30 ml) of 3,5-bis(2-pyridoxy)toluene (**L**₁**H**) (1.11 g, 4.0 mmol) and the mixture was refluxed for 24 h. The resultant mixture was cooled to room temperature, treated with 200 ml of deionized water and extracted with 3×30 ml of chloroform. The organic extracts were combined, dried over anhydrous MgSO₄, and evaporated to dryness to give crude [Pt(**L**₁)Cl] as an off-white solid. Colourless X-ray quality crystals were obtained by slow diffusion of diethylether into a solution of crude [Pt(**L**₁)Cl] (**1**) in chloroform. Yield 1.55 g, 76%. ¹H NMR (CDCl₃, 300 MHz) δ : 9.52 (dd, 2H, pyridoxyl-H), 7.88 (td, 2H, pyridoxyl-H), 7.27 (s, 2H, pyridoxyl-H), 7.05 (t, 2H, pyridoxyl-H), 6.82 (s, 2H, tolyl-H), 2.32 (s, 3H, tolyl-CH₃). ES-MS (CH₂Cl₂, +ve mode): 472 [M – Cl]⁺.

4.5. Synthesis of [Pt(**L**₂)Cl] (**2**)

[Pt(**L**₂)Cl] (**2**) was obtained in a similar way as **3** from K₂[PtCl₄] (1.66 g, 4.0 mmol) and 3,5-bis(2-pyridoxy)-2-dodecylbenzene (**L**₂**H**) (1.73 g, 4.0 mmol). Yield 1.60 g, 60%. ¹H NMR (CDCl₃, 300 MHz) δ : 9.44 (td, 2H, pyridoxyl-H), 7.85 (td, 2H, pyridoxyl-H), 7.04 (m, 2H, pyridoxyl-H), 6.89 (m, 2H, pyridoxyl-H), 6.60 (m, 1H, aryl-H), 6.55 (d, 1H, aryl-H), 6.50 (d, 1H, aryl-H), 1.27 (m, 25H, –C₁₂H₂₅). ES-MS (CH₂Cl₂, +ve mode): 626 [M – Cl]⁺.

4.6. Synthesis of [Pt(**L**₁)(CH₃CN)](ClO₄) (**3**)

[Pt(**L**₁)Cl] (**1**) (0.35 g, 0.7 mmol) was dissolved in acetonitrile (20 ml) and the resultant solution was stirred at room temperature for 8 h. LiClO₄ (0.1 g) was added and the mixture was further stirred at room temperature for an additional 0.5 h. Volume of the resultant acetonitrile solution was reduced to 10 ml under reduced pressure. Colourless X-ray quality crystals of

[Pt(L₁)(CH₃CN)](ClO₄) (**3**) were obtained by slow diffusion of diethylether into the acetonitrile solution. Yield 0.36 g, 84%. ¹H NMR (CDCl₃, 300 MHz) δ: 9.32 (dd, 2H, pyridoxyl-H), 8.20 (td, 2H, pyridoxyl-H), 7.52 (d, 2H, pyridoxyl-H), 7.32 (t, 2H, pyridoxyl-H), 6.88 (s, 1H, tolyl-H). ES-MS (CH₂Cl₂, +ve mode): 472 [M – CH₃CN]⁺.

4.7. Synthesis of {[Pt(L₁)₂(μ-dppm)](ClO₄)₂ (**4**)

A mixture of [Pt(L₁)Cl] (**1**) (0.25 g, 0.49 mmol) and dppm (94.0 mg, 0.25 mmol) in 1:1 acetonitrile/methanol (30 ml) was stirred for 12 h under a nitrogen atmosphere. The resultant mixture was filtered and evaporated under reduced pressure to about 10 ml. Addition of LiClO₄ (0.1 g) followed by slow diffusion of diethylether afforded {[Pt(L₁)₂(μ-dppm)](ClO₄)₂ (**4**) as colourless crystals. Yield 0.31 g, 85%. ¹H NMR (DMSO-d₆, 300 MHz) δ: 8.06–8.18 (m, 4H, pyridoxyl-H), 7.85–7.95 (m, 4H, pyridoxyl-H), 7.42–7.60 (m, 20H, –P(C₆H₅)₂), 7.31–7.36 (m, 4H, pyridoxyl-H), 7.03–7.12 (m, 4H, pyridoxyl-H), 6.88 (s, 4H, tolyl-H), 2.30 (m, 2H, –P(CH₂)P–), 1.92 (s, 6H, tolyl-CH₃). ³¹P NMR (DMSO-d₆, 300 MHz) δ: –8.78 (s, 2P, dppm). ES-MS (CH₂Cl₂, +ve mode): 856 [M – Pt(L₁)⁺, 472 [Pt(L₁)⁺.

4.8. Synthesis of {[Pt(L₂)₂(μ-dppm)](ClO₄)₂ (**5**)

{[Pt(L₂)₂(μ-dppm)](ClO₄)₂ (**5**) was obtained in a similar way as **4** from [Pt(L₂)Cl] (**2**) (0.30 g, 0.45 mmol) and dppm (86.0 mg, 0.23 mmol) as a pale pink oil after purification by silica gel column chromatography using dichloromethane/methanol (1:1) as eluent. Yield 0.25 g, 62%. ¹H NMR (DMSO-d₆, 300 MHz) δ: 8.07–8.26 (m, 4H, pyridoxyl-H), 7.66–7.90 (m, 4H, pyridoxyl-H), 7.19–7.66 (m, 20H, –P(C₆H₅)₂), 7.05–7.18 (m, 4H, pyridoxyl-H), 6.96–7.05 (m, 4H, pyridoxyl-H), 6.76–6.90 (m, 4H, tolyl-H), 2.10 (s, 2H, –P(CH₂)P–), 0.93–1.42 (s, 44H, –(CH₂)₁₁–), 0.74–0.92 (m, 6H, –CH₃). ³¹P NMR (DMSO-d₆, 300 MHz) δ: –8.78 (s, 2P, dppm). ES-MS (DMSO, +ve mode): 1637 [M]⁺.

4.9. Synthesis of {[Pt(L₁)₂(μ-pyrazole)](ClO₄) (**6**)

A mixture of [Pt(L₁)Cl] (**1**) (0.25 g, 0.49 mmol), pyrazole (16.7 mg, 0.25 mmol) and potassium *tert*-butoxide (28.0 mg, 0.25 mmol) in 2:1 acetonitrile/methanol (30 ml) was refluxed for 12 h under a nitrogen atmosphere. LiClO₄ (0.1 g) was then added and the resultant mixture was further stirred at room temperature for an additional 0.5 h. The mixture was evaporated under reduced pressure to about 10 ml and filtered. Slow diffusion of diethylether into the resultant solution afforded {[Pt(L₁)₂(μ-pyrazole)](ClO₄) (**6**) as colourless X-ray

quality crystals. Yield 0.16 g, 58%. ¹H NMR (DMSO-d₆, 300 MHz) δ: 7.80 (d, 2H, pyrazolyl-H), 7.60–7.67 (m, 4H, pyridoxyl-H), 7.42–7.45 (m, 4H, pyridoxyl-H), 7.04–7.10 (m, 4H, pyridoxyl-H), 6.74–6.82 (m, 4H, pyridoxyl-H), 6.79 (s, 4H, tolyl-H), 6.70 (t, 1H, pyrazolyl-H), 2.37 (s, 6H, tolyl-CH₃). ES-MS (DMSO, +ve mode): 1011 [M]⁺.

4.10. Synthesis μ of {[Pt(L₂)₂(-pyrazole)](ClO₄) (**7**)

{[Pt(L₂)₂(μ-pyrazole)](ClO₄) (**7**) was obtained in a similar way as **6** from [Pt(L₂)Cl] (**2**) (0.25 g, 0.38 mmol) and pyrazole (12.9 mg, 0.19 mmol) as a pale pink oil after purification by silica gel column chromatography using dichloromethane/methanol (1:1) as eluent. Yield 0.11 g, 41%. ¹H NMR (DMSO-d₆, 300 MHz) δ: 8.20 (m, 4H, pyridoxyl-H), 7.94 (s, 1H, pyrazolyl-H), 7.78–7.89 (m, 4H, pyridoxyl-H), 7.43–7.56 (m, 4H, pyridoxyl-H), 7.11–7.25 (m, 4H, tolyl-H), 6.97 (d, 2H, pyrazolyl-H), 6.72–6.96 (m, 4H, pyridoxyl-H), 1.00–1.46 (m, 44H, –(CH₂)₁₁–), 0.84 (t, 6H, –CH₃). ES-MS (DMSO, +ve mode): 1320 [M]⁺.

4.11. Synthesis of {[Pt(L₁)₂(μ-imidazole)](ClO₄) (**8**)

{[Pt(L₁)₂(μ-imidazole)](ClO₄) (**8**) was obtained in a similar way as **6** from [Pt(L₁)Cl] (**1**) (0.25 g, 0.49 mmol), imidazole (16.7 mg, 0.25 mmol) and potassium *tert*-butoxide (28.0 mg, 0.25 mmol). Colourless X-ray quality crystals of **8** were obtained by slow diffusion of diethylether into an acetonitrile solution of **8**. Yield 0.14 g, 50%. ¹H NMR (DMSO-d₆, 300 MHz) δ: 8.17 (td, 4H, pyridoxyl-H), 7.90 (s, 1H, imidazolyl-H), 7.73 (dd, 4H, pyridoxyl-H), 7.57 (dd, 4H, pyridoxyl-H), 7.31 (s, 2H, imidazolyl-H), 7.26 (td, 4H, pyridoxyl-H), 6.93 (s, 4H, tolyl-H), 2.32 (s, 6H, tolyl-CH₃). ES-MS (DMSO, +ve mode): 1011 [M]⁺.

4.12. Synthesis of {[Pt(L₂)₂(μ-imidazole)](ClO₄) (**9**)

{[Pt(L₂)₂(μ-imidazole)](ClO₄) (**9**) was obtained in a similar way as **6** from [Pt(L₂)Cl] (**2**) (0.25 g, 0.38 mmol) and imidazole (12.9 mg, 0.19 mmol) as a pale pink oil after purification by silica gel column chromatography using dichloromethane/methanol (1:1) as eluent. Yield 0.10 g, 37%. ¹H NMR (DMSO-d₆, 300 MHz) δ: 8.20 (m, 4H, pyridoxyl-H), 7.85 (s, 1H, imidazolyl-H), 7.76 (dd, 4H, pyridoxyl-H), 7.60 (td, 4H, pyridoxyl-H), 7.20–7.40 (m, 2H, imidazolyl-H and 4H, tolyl-H), 7.02 (m, 4H, pyridoxyl-H), 1.00–1.46 (s, 44H, –(CH₂)₁₁–), 0.84 (t, 6H, –CH₃). ES-MS (DMSO, +ve mode): 1320 [M]⁺.

Table 4

Crystallographic data for [Pt(L₁)Cl] (**1**), [Pt(L₁)(CH₃CN)](ClO₄) (**3**), {[Pt(L₁)₂(μ-pyrazole)](ClO₄) (**6**) and {[Pt(L₁)₂(μ-imidazole)](ClO₄)·2CH₃CN (**8**)·2CH₃CN

Complex	1	3	6	8
Formula	C ₁₇ H ₁₃ N ₂ ClO ₂ Pt	C ₁₉ H ₁₆ N ₃ ClO ₆ Pt	C ₃₇ H ₂₉ N ₆ ClO ₈ Pt ₂	C ₄₁ H ₃₅ N ₈ ClO ₈ Pt ₂ ·2CH ₃ CN
Formula mass	507.83	612.89	1111.29	1193.40
Crystal system	Hexagonal	Monoclinic	Triclinic	Triclinic
Space group	<i>R</i> 3̄	<i>P</i> 2 ₁ / <i>c</i>	<i>P</i>	<i>P</i>
<i>a</i> (Å)	46.610(3)	25.668(2)	12.7171(6)	8.9990(13)
<i>b</i> (Å)	46.610(3)	7.3647(6)	15.5140(7)	14.692(2)
<i>c</i> (Å)	4.0755(4)	24.250(2)	19.7552(9)	16.660(2)
α (°)	90	90	77.9150(10)	86.873(3)
β (°)	90	117.3090(10)	71.9270(10)	84.247(3)
γ (°)	120	90	88.5800(10)	73.486(3)
<i>U</i> (Å ³)	7667.6(10)	4073.2(6)	3619.8(3)	2077.1(5)
<i>Z</i>	18	8	4	2
<i>T</i> (K)	293	293	293	293
<i>F</i> (000)	4320	2352	2120	1148
<i>D</i> _{calc} [mg cm ⁻³]	1.980	1.999	2.039	1.908
μ (Mo Kα) [mm ⁻¹]	8.401	7.063	7.857	6.855
Reflection collected	12,812	19,068	21,560	12,614
Unique reflections	2994	7160	15,615	9157
<i>R</i> _{int}	0.0549	0.0577	0.0174	0.0389
Observed reflections	2366	6131	12134	5079
GOF on <i>F</i> ²	0.950	1.028	0.791	0.872
<i>R</i> ₁ , <i>wR</i> ₂ [<i>I</i> > 2.0σ <i>I</i>]	0.0539, 0.1460	0.0489, 0.1304	0.0266, 0.0622	0.0475, 0.1003

4.13. X-ray crystallographic studies

Geometric and intensity data of complex **1**, **3**, **6** and **8** were collected on a Bruker Axs SMART 1000 CCD area-detector using graphite monochromated Mo Kα radiation (λ = 0.71073 Å). The collected frames were processed with the software SAINT [16] and an absorption correction was applied (SADABS [17]) to the collected reflections. The structure was solved by direct methods (SHELXTL [18]) in conjunction with standard difference Fourier techniques and subsequently refined by full-matrix least-square analyses on *F*². All non-hydrogen atoms were assigned with anisotropic displacement parameters. The hydrogen atoms were generated in their idealized positions and allowed to ride on the respective carbon atoms. Crystal data and other experimental details are given in Table 4.

CCDC-201591 to 201594 contains the supplementary crystallographic data for this paper. These data can be obtained free of charge at www.ccdc.cam.ac.uk/conts/retrieving.html [or from the Cambridge Crystallographic Data Centre, 12, Union Road, Cambridge CB2 1EZ, UK; fax: (internat.) +44-1223/336-033; e-mail: deposit@ccdc.cam.ac.uk].

Acknowledgements

The work described in this paper was jointly funded by a grant from the Research Grants Council of Hong Kong SAR, China (CityU 1108/02P) and a Grant from CityU (Project No. 7001281).

References

- [1] (a) P. Steenwinkel, R.A. Gossage, G. van Koten, Chem. Eur. J. 4 (1998) 759–762; (b) B. Rybtchinsky, D. Milstein, Angew. Chem., Int. Ed. Engl. 38 (1999) 870–883; (c) C.M. Jensen, Chem. Commun. (1999) 2443–2449; (d) M. Albrecht, G. van Koten, Angew. Chem. Int. Ed. 40 (2001) 3750–3781; (e) M. Albrecht, B.M. Kocks, A.L. Spek, G. van Koten, J. Organomet. Chem. 624 (2001) 271–286; (f) B.M.J.M. Suijkerbuijk, M.Q. Slagt, R.J.M.K. Gebbink, M. Lutz, A.L. Spek, G. van Koten, Tetrahedron Lett. 43 (2002) 6565–6568; (g) G. Rodríguez, M. Lutz, A.L. Spek, G. van Koten, Chem. Eur. J. 8 (2002) 45–57; (h) D. Morales-Morales, R.E. Cramer, C.M. Jensen, J. Organomet. Chem. 654 (2002) 44–50; (i) J.T. Singleton, Tetrahedron 59 (2003) 1837–1857; (j) M.E. van der Boom, D. Milstein, Chem. Rev. 103 (2003) 1759–1792; (k) D.W. Lee, C.M. Jensen, D. Morales-Morales, Organometallics 22 (2003) 4744–4749.
- [2] (a) C.S. Peyratout, T.K. Aldridge, D.K. Crites, D.R. McMillin, Inorg. Chem. 34 (1995) 4484–4489; (b) L.Z. Wu, T.C. Cheung, C.M. Che, K.K. Cheung, M.H.W.

- Lam, Chem. Commun. (1998) 1127–1128;
- (c) K.H. Wong, M.C.W. Chan, C.M. Che, Chem. Eur. J. 5 (1999) 2845–2849;
- (d) M. Albrecht, R.A. Gossage, M. Lutz, A.L. Spek, G. van Koten, Chem. Eur. J. 6 (2000) 1431–1445.
- [3] (a) J. Buey, P. Espinet, J. Organomet. Chem. 507 (1996) 137–145;
- (b) M. Ghedini, D. Pucci, A. Crispini, G. Barberio, Organometallics 18 (1999) 2116–2124;
- (c) W. Lu, B.X. Mi, M.C.W. Chan, Z. Hui, N. Zhu, S.T. Lee, C.M. Che, Chem. Commun. (2002) 206–207;
- (d) G. Rodríguez, M. Albrecht, J. Schoenmaker, A. Ford, M. Lutz, A.L. Spek, G. van Koten, J. Am. Chem. Soc. 124 (2001) 5127–5138;
- (e) C. Adachi, M.A. Baldo, S.R. Forrest, S. Lamansky, M.E. Thompson, Appl. Phys. Lett. 78 (2001) 1622–1624;
- (f) J.W. Slater, D.P. Lydon, J.P. Rourke, J. Organomet. Chem. 645 (2002) 246–255;
- (g) P. Espinet, J. Etxebarria, C.L. Folicca, J. Ortega, M.B. Ros, J.L. Serrano, Adv. Mater. 8 (1996) 745–748;
- (h) J. Buey, L. Dez, P. Espinet Kitzerow, H.-S. Kitzerow, J.A. Miguel, Chem. Mater. 8 (1996) 2375–2381.
- [4] (a) C.W. Chan, T.F. Lai, C.M. Che, S.M. Peng, J. Am. Chem. Soc. 115 (1993) 11245–11253;
- (b) C.W. Chan, L.K. Cheng, C.M. Che, Coord. Chem. Rev. 132 (1994) 87–97;
- (c) D.J. Cárdenas, A.M. Echavarren, Organometallics 18 (1999) 3337–3341.
- [5] (a) M. Maestri, C. Deuschel-Cornioley, A. von Zelewsky, Coord. Chem. Rev. 111 (1991) 117–123;
- (b) G.W.V. Cave, F.P. Fanizzi, R.J. Deeth, W. Errington, J.P. Rourke, Organometallics 19 (2000) 1355–1364.
- [6] (a) V.H. Houlding, V.M. Miskowski, Coord. Chem. Rev. 111 (1991) 145–152;
- (b) V.M. Miskowski, V.H. Houlding, Inorg. Chem. 30 (1991) 4446–4452;
- (c) S.W. Lai, H.W. Lam, W. Lu, K.K. Cheung, C.M. Che, Organometallics 21 (2002) 226–234;
- (d) S.W. Lai, M.C.W. Chan, T.C. Cheung, S.M. Peng, C.M. Che, Inorg. Chem. 38 (1999) 4046–4055.
- [7] C.M. Hartshorn, P.J. Steel, Inorg. Chem. 35 (1996) 6902–6903.
- [8] R. Romeo, M.R. Plutino, L.M. Scolaro, S. Stoccore, G. Minghetti, Inorg. Chem. 39 (2000) 4749–4755.
- [9] J.S. Fossey, C.J. Richards, Organometallics 21 (2002) 5259–5264.
- [10] H.K. Yip, C.M. Che, Z.Y. Zhou, T.C.W. Mak, J. Chem. Soc. Chem. Commun. (1992) 1369–1370.
- [11] T.C. Cheung, K.K. Cheung, S.M. Peng, C.M. Che, J. Chem. Soc., Dalton Trans. (1996) 1645–1652.
- [12] J.A. Bailey, V.M. Miskowski, H.B. Gray, Inorg. Chem. 32 (1993) 369–370.
- [13] E. Pretsch, W. Simon, J. Seibol, J. Clerc, Tables of Spectral Data for Structure Determination of Organic Compounds, in: W. Fresenius, J.F.K. Huber, E. Pungor, G.A. Rechnitz, W. Simon, Th.S. West (Eds.), Chemical Laboratory Practices, second ed., Springer-Verlag, Berlin, 1989.
- [14] W. Lu, M.C.W. Chan, K.K. Cheung, C.M. Che, Organometallics 20 (2001) 2477–2486.
- [15] J.A. Bailey, M.G. Hill, R.E. Marsh, V.M. Miskowski, W.P. Schaefer, H.B. Gray, Inorg. Chem. 34 (1995) 4591–4599.
- [16] SAINT, Reference manual, Siemens Energy and Automation, Madison, WI, 1994–1996.
- [17] G.M. Sheldrick, SADABS, Empirical Absorption Correction Program, University of Göttingen, Germany, 1997.
- [18] G.M. Sheldrick, SHELXTL™, Reference Manual, Version 5.1, Siemens, Madison, WI, 1997.